V838 Monocerotis: the central star and its environment a decade after outburst

Olivier Chesneau, Florentin Millour, Orsola De Marco, S.N. Bright, Alain Spang, D. P. K. Banerjee, N. M. Ashok, T. Kaminski, John P. Wisniewski, Anthony Meilland, et al.

V838 Monocerotis: the central star and its environment a decade after outburst

O. Chesneau[1,†], F. Millour[1], O. De Marco[2], S. N. Bright[1,2], A. Spang[1], D. P. K. Banerjee[3], N. M. Ashok[3], T. Kamiński[4], J P. Wisniewski,[5], A. Meilland[1], and E. Lagadec[1] [*]

[1] Laboratoire Lagrange, UMR7293, Univ. Nice Sophia-Antipolis, CNRS, Observatoire de la Côte d'Azur, 06300 Nice, France
[2] Department of Physics & Astronomy, Macquarie University, Sydney, NSW 2109, Australia
[3] Physical Research Laboratory, Navrangpura, Ahmedabad, Gujarat, India
[4] Max-Planck Institut für Radioastronomie, Auf dem Hügel 69, D-53121 Bonn, Germany
[5] HL Dodge Department of Physics & Astronomy, University of Oklahoma, 440 W Brooks Street, Norman, OK 73019, USA

Received, accepted.

ABSTRACT

Aims. V838 Monocerotis erupted in 2002, brightened in a series of outbursts, and eventually developed a spectacular light echo. A very red star emerged a few months after the outburst. The whole event has been interpreted as the result of a merger.
Methods. We obtained near-IR and mid-IR interferometric observations of V838 Mon with the AMBER and MIDI recombiners located at the Very Large Telescope Interferometer (VLTI) array. The MIDI two-beam observations were obtained with the 8m Unit Telescopes between October 2011 and February 2012. The AMBER three-beam observations were obtained with the compact array (B≤35m) in April 2013 and the long array (B≤140m) in May 2014, using the 1.8m Auxiliary Telescopes.
Results. A significant new result is the detection of a compact structure around V838 Mon, as seen from MIDI data. The extension of the structure increases from a FWHM of 25 mas at 8 μm to 70 mas at 13 μm. At the adopted distance of $D = 6.1 \pm 0.6$ kpc, the dust is distributed from about 150 to 400 AU around V838 Mon. The MIDI visibilities reveal a flattened structure whose aspect ratio increases with wavelength. The major axis is roughly oriented around a position angle of $-10°$, which aligns with previous polarimetric studies reported in the literature. This flattening can be interpreted as a relic of the 2002 eruption or by the influence of the currently embedded B3V companion. The AMBER data provide a new diameter for the pseudo-photosphere, which shows that its diameter has decreased by about 40% in 10yrs, reaching a radius $R_* = 750 \pm 200$ $R_\odot$ (3.5 ± 1.0 AU).
Conclusions. After the 2002 eruption, interpreted as the merging of two stars, it seems that the resulting source is relaxing to a normal state. The nearby environment exhibits an equatorial over-density of dust up to several hundreds of AU.

Key words. Techniques: high angular resolution; individual: V838 Mon; Stars: circumstellar matter; Stars: mass-loss

1. Introduction

V838 Mon is a nova-like object, which erupted in 2002 in a series of outbursts (reaching V∼6.8). It subsequently developed a light echo which was extensively studied by Bond et al. (2003); Banerjee et al. (2006); Tylenda & Kamiński (2012). The eruption was unlike classical novae as the effective temperature of the object dropped and the spectral type evolved into a very late L-type supergiant (Evans et al. 2003; Loebman et al. in press). The event has been interpreted as the merger of a ∼8 M$_\odot$ star with a sub-solar mass star (Soker & Tylenda 2003; Tylenda et al. 2005; Tylenda & Soker 2006). The mid infrared flux of V838 Mon increased by a factor of two between 2004 and 2007, suggesting that new dust was forming in the expanding ejecta of the outbursts (Wisniewski et al. 2003a; Tylenda 2005; Wisniewski et al. 2008). The expanding ejecta engulfed a companion close to the central source (Bond 2006; Munari et al. 2007; Kolka et al. 2009).

The progenitor of V838 Mon was found in a variety of surveys, including 2MASS, and appears consistent with a somewhat reddened early main sequence star. Post-outburst observations have found a faint, blue component in the spectrum and Tylenda et al. (2005) argued that the pre-outburst spectral energy distribution (SED) is well-matched by a pair of early main sequence stars (B3V + B1.5V or B4V + A0.5V), making V838 Mon a triple system *de facto* (main star + sub-solar merging star + B3V companion). Lynch et al. (2004) obtained numerous IR spectra of V838 Mon during and after the eruption (2002-2003). They fit their data to a model consisting of a cool (T$_{eff}$ = 2100K, R$_*$ = 8.8 AU) stellar photosphere surrounded by a large, absorbing molecular cloud. A more recent work (Loebman et al. in press) provides precise estimates of the stellar and enshrouding cloud parameters, with an effective temperature of the star of 2000–2200 K, and a radius of the shell of $R = 263 \pm 10$ AU.

Lane et al. (2005) first used long-baseline near-IR (2.2 μm baselines smaller than 85 m) interferometry in November-December 2004 to provide the first direct measurement of the angular size of V838 Mon using the two-telescope recombiner Palomar Testbed Instrument (PTI). At this epoch, they measured an angular diameter for the central source of $\Theta = 1.83 \pm 0.06$ mas. Reasonably accurate distances were determined from the light echo and using other methods (Munari et al. 2005;

Sparks et al. 2008; Kamiński et al. 2011). We adopt the distance $D = 6.1 \pm 0.6$ kpc from Sparks et al. (2008). Using this distance, the interferometric diameter translates to a linear radius for the supergiant of 1200 ± 150 R$_\odot$ (5.6 ± 0.7 AU). Lane et al. (2005) could also fit the data assuming an elliptical structure with a major axis oriented at P.A. 15° whose extensions are 3.57×0.07 mas (i.e. the minor axis is unresolved).

V838 Mon is embedded in a dense, large scale environment (Tylenda & Kamiński 2012; Kamiński et al. 2011; Exter et al. 2014), potentially contaminating observations of the central star. High angular resolution studies with a field-of-view (FOV) of a few arcsec are an asset in that domain to isolate the central regions from the extended dusty cloud. A great advantage of optical interferometry studies is to fully isolate the measurements from the extended environment.

This letter presents optical interferometry measurements obtained with the Very Large Telescope Interferometer (VLTI). The observations are presented in Sect. 2. In Sect. 3 we analyze the MIDI mid-IR measurements followed by the AMBER K band measurements by means of simple geometrical models. The results are then discussed in Sect. 4.

2. Observations

Mid-IR interferometric data were obtained with the two-telescope recombiner MIDI (Leinert et al. 2004) between October 2011 and February 2012 using the 8m Unit Telescopes (UTs) of the Very Large Telescope. These observations provided dispersed fringe visibilities between 8 and 13 μm in addition to classical spectrophotometric capabilities.

Near-infrared observations were obtained with AMBER (a three-telescopes combiner located at the VLTI: Petrov et al. 2007) in November 2012 and February 2013, using the low spectral resolution mode (R=35) with the UTs. Unfortunately, these data are unusable due to a bad calibrator (see details in appendix A) and therefore not presented here. In April 2013, observations were repeated with the 1.8m Auxiliary Telescopes (ATs) under photometric conditions, using the compact configuration ($B \leq 35$m) and more suitable calibrators. The extended configuration ($B \leq 140$m) was subsequently used in May 2014 to observe V838 Mon.
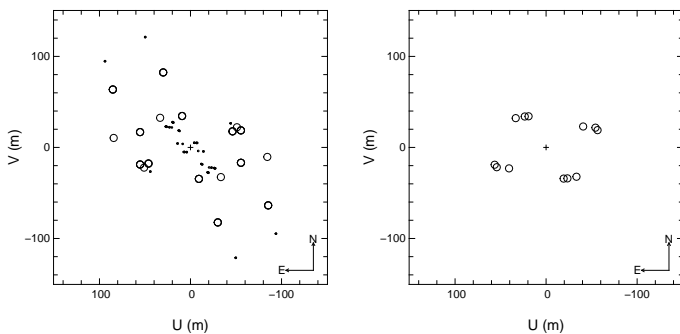

Fig. 1. Left: (u, v) coverage of the AMBER observations. Small dots are observations with ATs and larger circles with UTs. **Right:** (u, v) coverage of the MIDI observations.

The great advantage of both instruments is that the FOV of the interferometric measurements are within the point spread function of a single telescope, i.e. the same value of ~0.3" at 2.2 μm for the 1.8m ATs with AMBER, and at 10 μm for the 8m

UTs with MIDI. This isolates the central source from the extended emission of the cloud in which V838 Mon is embedded. The observation log is presented in Table 1 and the (u, v) plane coverage is plotted in Fig.1.

We reduced the AMBER data using the standard data reduction software `amdlib v3.0.8` (Tatulli et al. 2007; Chelli et al. 2009). Near-infrared JHK photometry was obtained on a regular basis from the 1.2m telescope at the Mt. Abu Observatory, India (Banerjee & Ashok 2012). These measurements helped to prepare the interferometric observations. On March 1, 2013, the J, H, K band magnitudes were 7.12, 5.91, 5.43, respectively, almost unchanged since November 2011.

Table 1. Log of AMBER and MIDI observations of V838 Mon.

Date	Stations	Calibrators	Wavelength	Nb. obs.
MIDI				
10/10/2011	U3-U4	1°	8–13 μm	2
13/12/2011	U2-U3	1°	8–13 μm	1
14/12/2011	U2-U3	1°	8–13 μm	1
11/02/2012	U3-U4	1°	8–13 μm	1
AMBER				
14/04/2013	A1-B2-D0	6◁, 7▷	1.54–2.50 μm	3
15/04/2013	A1-C1-D0	6◁, 8△	1.56–2.50 μm	2
06/05/2014	A1-G1-J3	9▽	1.53–2.46 μm	1

Notes. Calibrator angular diameters from SearchCal/JMMC (Bonneau et al. 2006) and getCal/NExScI. °: HD 52666 2.53 ± 0.21 mas, ◁: HD 52265 0.44 ± 0.03 mas, ▷: HD 64616 0.51 ± 0.04 mas, △: HD 63660 0.96 ± 0.07 mas, ▽: HD 54990 0.57 ± 0.59 mas.

Visibilities are a proxy to the object's size and shape. The AMBER visibilities are presented in Fig. 2 at selected wavelengths for all baselines, and for the longest baseline in Fig. 3 together with the JHK Mt. Abu spectrum. Strong variations as a function of wavelength are seen, especially at the edge of the H and K bands where they decrease relative to the bands centers (1.7 μm and 2.2 μm). All baseline lengths show this curved shape. We are confident this is not a flux bias or instrumental effect, but comes from the source itself.

Closure phases can be qualitatively interpreted as a proxy to asymmetries: a non-zero (modulo π) closure phase is a sign of asymmetries in the object's shape. The 2014 closure phases are of good quality and compatible with zero with a mean value of $-1°04 \pm 1°12$. The object is therefore likely centro-symmetric as seen by AMBER. The spectral-range of the AMBER data is 1.5–2.5 μm.

The MIDI data were processed using the `MIA+EWS` software[1] (Chesneau 2007). The data were secured in High_Sens mode implying that the photometry is obtained subsequently to fringes. The quality of the data ranges from high quality (error level ~10%) to poor quality for some baselines (error level reaching ~25%). The spectrophotometric calibration of the mid-IR flux was performed with the calibrator HD 52666 (M2III, IRAS F12=18.3 Jy with a 5% error). The ten MIDI spectra from two telescopes were merged leading to a spectrophotometry with an 8% error level, representing the mid-IR flux of the source between October and February 2011. The spectrum was compared with measurements at the same epoch from the WISE[2] and AKARI[3] satellites obtained with much larger apertures. The

---

[1] http://home.strw.leidenuniv.nl/~nevec/MIDI/

[2] taken in April 2 and October 10, 2010

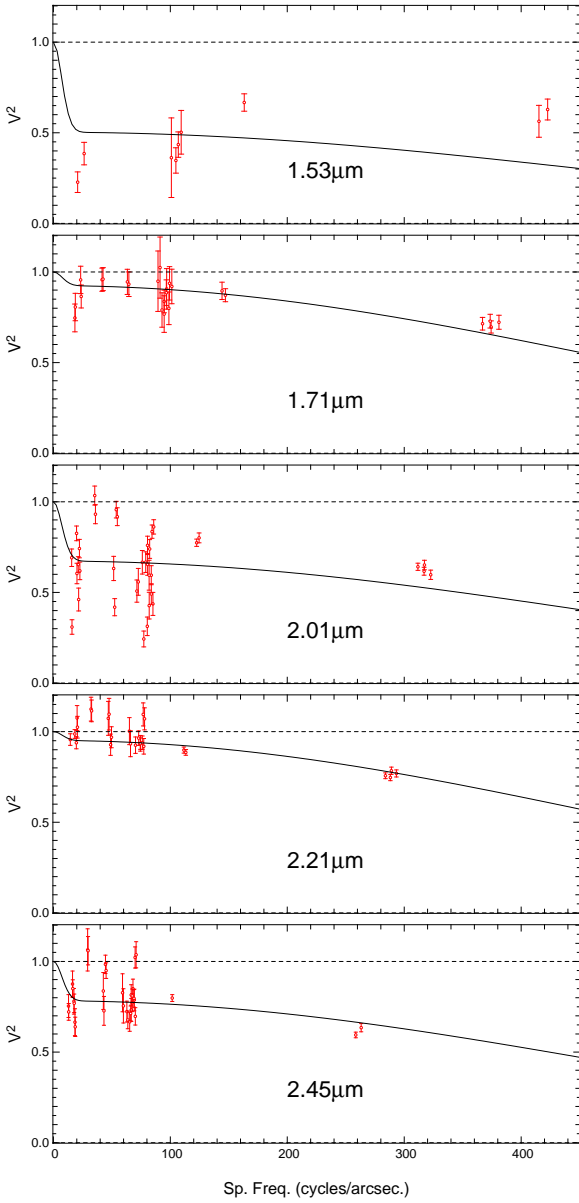[3] obtained between May 2006 and August 2007

Fig. 2. AMBER data shown as a function of spatial frequencies for selected wavelengths. The black line shows our best-fit model of a uniform disk plus an extended component (50 mas FWHM here).

flux in the WISE filter ($\lambda = 11.56\,\mu$m, $\Delta\lambda = 5.51\,\mu$m) is 31.56 ± 0.06 Jy and in the AKARI filter ($\lambda = 8.22\,\mu$m, $\Delta\lambda = 4.10\,\mu$m) the flux is 20.11 ± 0.39 Jy. The spectrophotometry and the corresponding Gaussian estimates from the MIDI are shown in Fig. 4.

3. Analysis

The MIDI dispersed visibilities were translated to the simplest possible geometrical ad-hoc model – a Gaussian brightness distribution, as described in Leinert et al. (2004). The resulting fits shown in Fig. 4 depict the general appearance of the mid-infrared structure. The semi-major and semi-minor axes of the drawn ellipses represent the half-width at half maximum (HWHM) of the Gaussian. The extent of that structure increases from a FWHM of 25 mas at $8\,\mu$m to 70 mas at $13\,\mu$m, with a high flattening ratio. Despite the heterogeneity of the quality of the MIDI visibilities,
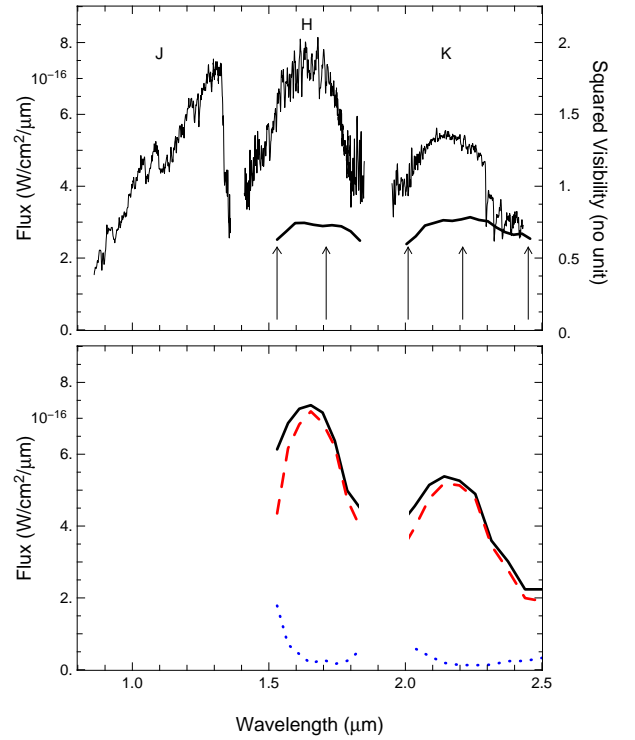

Fig. 3. Top: The 0.85–2.5 micron spectrum of V838 Mon on 11 December 2013 corrected for extinction using E(B-V) = 0.5. For comparison, we show the AMBER longest baseline visibility (thick black lines, right axis), and indicate with arrows the wavelengths of Fig. 2. **Bottom:** Spectra extracted from the AMBER data according to a downgraded resolution version of the above spectrum (black line). Red dashed line: the star spectrum. Blue dotted line: extended emission spectrum.

the flattening of that structure is certain, but we can only provide a loose range for flattening ratio values between 1.1 and 2.5 near $9\,\mu$m, and between 1.3 and 60 near $12\,\mu$m. The major axis is oriented at a P.A. close to $-10°$ with an uncertainty of more than $\pm30°$. The flattening increases with the wavelength, from a roughly round structure at $8\,\mu$m to a very flattened structure at $13\,\mu$m. This may come from the contribution of the star, stronger at $8\,\mu$m. The flux from WISE agrees fairly well with the MIDI flux. AKARI data is offset in time from the MIDI data by 5 to 6 years. Given that the source's SED has been evolving in the IR (Wisniewski et al. 2008) it is not unexpected or surprising that there is some difference in the value of the 9 micron flux measured by AKARI and MIDI. This implies that most of the mid-IR flux in 2011 originates from the vicinity of the central star (≤ 0.4").

The 2013 short-baseline AMBER visibilities are all very close to unity in the band centers at $1.7\,\mu$m and $2.2\,\mu$m and are consistent with a completely unresolved object. The long-baseline, 2014 visibilities are close to $V^2 = 0.8$ at the same wavelengths.

The visibilities as a function of wavelength of the *H* and *K* bands decrease relative to the bands centers ($1.7\,\mu$m and $2.2\,\mu$m), as shown in Fig. 3. This is indicative of an object whose shape changes as a function of wavelength. At the same time, the visibilities at the edge of the bands ($1.5\,\mu$m, $2.0\,\mu$m and $2.4\,\mu$m) show a "plateau-like" shape as a function of spatial frequencies (see Fig. 2), indicative of an additional resolved component. We therefore analysed first the *K* band center using a single-

component model, and then added an additional component to analyze the full AMBER dataset.
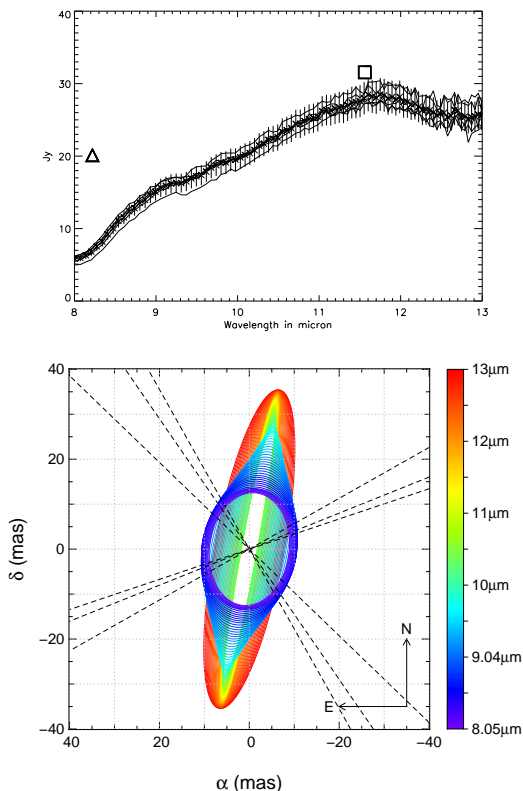

Fig. 4. Top: MIDI spectrum obtained in 2011. We added for comparison AKARI (triangle) and WISE (square) fluxes. **Bottom:** 2D Gaussian fit to the whole MIDI dataset. The dashed lines represent the direction of the observation baselines.

We used the `fitOmatic` software (Millour et al. 2009) to derive an angular diameter assuming a uniform disk model around $2.2\mu m$. If we include all the 2013 (short baselines) and 2014 (long baselines) observations, we find a diameter of 1.17 ± 0.37 mas. If we keep only the 2014 data, we obtain a diameter of 1.15 ± 0.20 mas. We adopt the latter diameter of 1.15 ± 0.20 mas as the 2013 data (short baselines) do not resolve the central star. This measured diameter is significantly smaller than the one published by Lane et al. (2005).

The AMBER closure phases are all equal to zero within the error bars. We can therefore constrain the flux of an hypothetical companion star in addition to the central merger. To achieve that, we added a point-source to our model and used a simulated annealing algorithm to constrain its parameters using the observed visibilities and closure phases and starting with random initial parameters. Our conclusion is that its flux was always smaller than 3% of the total flux, i.e. there would be at minimum 4 magnitudes difference between primary and secondary companion. The AMBER observations do not exclude the presence of the companion, but put important constraints on its NIR contribution to the SED.

The decreasing visibilities at the edges of the H and K bands indicate the presence of extended emission with a varying spectrum (as shown in lower panel in Fig. 3, blue dotted line). We cannot constrain the exact size of this contribution due to the plateau-like shape of visibilities as a function of spatial frequen-

cies, but we can provide a lower limit of its size of $\theta \geq 20$ mas. We tentatively associate this emission to the MIDI elongated dusty structure. The extended component would correspond to the H and K bands contribution of the MIDI elongated structure. It is noteworthy that adding this additional source of emission does not significantly change the estimated diameter for the central star.

To complement these measurements, we used a JHK spectrum of the star from Mt Abu (India), obtained on 11 December 2013, to derive a low-resolution spectrum of the central star and the extended emission (Fig. 3, lower panel). The stellar spectrum is typical of a cool luminous star (see Lançon & Wood 2000; Banerjee & Ashok 2002, for a comparison) with prominent first overtone CO bands at $2.29\mu m$ and beyond. Similar, albeit weak, CO second overtone features are also seen in the H band. The deep down-turns at the band edges are due to the presence of water in its atmosphere (Banerjee et al. 2005). Other molecular features of VO and TiO are also seen, including some rather uncommon bands of AlO. The spectrum of the extended structure shows emission bands at the H and K band edges, where the water absorption occurs in the total spectrum.

4. Discussion

The P.A. of the major axis, as inferred from the dusty flattened structure discovered by MIDI is $\approx -10°$. The MIDI size increase is expected for a non-truncated dusty disk. At the adopted distance, the dust is distributed between 150 and 400 AU from V838 Mon. Such findings are also in agreement with the earliest accurate spectropolarimetric measurements reported by Wisniewski et al. (2003a,b). They reported an intrinsic polarisation with a P.A. of $127°.0 \pm 0°.5$ interpreted as scattering by a disk with a major axis at a P.A. of $37°$.

The 2004 PTI interferometric data had been interpreted as either a uniform disk or an elliptical model, both consistently explaining the data well. We note that the P.A.$=15^{+3}_{-27}°$ derived from PTI is roughly aligned with our longest AMBER baselines, i.e. we would be sensitive to the major axis size in case the correct Lane et al. (2005) model had been that of an elongated structure. Our AMBER data suggest a different picture. The supergiant has decreased in angular size by $\approx 40\%$ in ≈ 10 years since the measurements of Lane et al. (2005). The linear radius is now estimated to 750 ± 200 $R_\odot$ (3.5 ± 1.0 AU). Such a radius is comparable to the famous M2 Iab supergiant Betelgeuse (Haubois et al. 2009, 885 ± 90 $R_\odot$). Such an evolution has already been suggested by (Geballe et al. 2007). This diameter decrease means the star's photosphere has shrinked during the intervening period at an approximate rate of $1 km\,s^{-1}$.

The good quality of the closure phases provides crucial constraints and excludes any secondary star brighter than a few percent of the total flux in the 6–600 AU separation range. Yet, we caution that a B3V star whose K band magnitude is fainter than 15 would be totally undetectable by the interferometer.

The AMBER interferometric observations obtained 10 yr after PTI suggest a contraction of the central star by about 40%, which is in line with the spectral change of V838 Mon toward a 'normal' M-type supergiant. No clear sign of deformation of the photosphere is detected.

The extended emission found in the AMBER data is enhanced relative to the central star around the CO overtone absorption features and the H_2O absorption at the band edges. This means there is water emission around the star at an angular scale larger than 20 mas, and smaller than 250 mas (field of view of

one telescope at $2.2\,\mu$m). We tentatively associate this emission to the MIDI elongated dusty structure.

Several hypotheses could be proposed to explain the detection of the flattened structure at large distance, as observed by MIDI and supported by AMBER.

The most likely hypothesis is that the flattened structure is simply the relic of the large dust formation event as a consequence of the merging of the two stars (Wisniewski et al. 2008, 2003a; Nicholls et al. 2013). The ejecta velocity was low at outburst time – less than $200\,\mathrm{km\,s^{-1}}$ as derived from P-Cygni profiles by Lynch et al. (2004) from several lines. In the 10 years since outburst, ejected material would not have travelled beyond 400 AU. This scenario is compatible with our finding.

The interferometric observations may also be discussed in the context of the B3V companion discovered around V838 Mon (Desidera & Munari 2002; Wagner & Starrfield 2002; Munari et al. 2002, 2005) and observed in the post-outburst spectra. The presence of the companion would explain the X-ray activity discovered in the vicinity of V838 Mon (Antonini et al. 2010). It is important to note that the distance of this companion from the central star was investigated by Munari et al. (2007), and they estimated the minimum separation to about 28 AU. On the other hand, Tylenda et al. (2009) derived a separation of $\approx$ 250 AU. This is well within the separation range detectable by AMBER. The MIDI measurements suggest a large separation of about 100 AU. In 2009, the B3V hot signature was no longer observed (Kolka et al. 2009). We would propose then that the companion is building a circumbinary disk via the Lagrangian point L2, as proposed in some observational and theoretical studies on other sources (Plets et al. 1995; Meilland et al. 2010; Millour et al. 2011).

To conclude, we find a flattened dusty structure around V838 Mon. We also find that the central star decreased its diameter by nearly 40% in 10 years.

The interferometric picture of V838 Mon as of today is the following: it is now slowly becoming an anonymous red supergiant, surrounded by a flattened, probably transitory, dusty environment extending up to several hundreds of AU.

References

Antonini, F., Montez, Jr., R., Kastner, J. H., et al. 2010, ApJ, 717, 795
Banerjee, D. P. K. & Ashok, N. M. 2002, A&A, 395, 161
Banerjee, D. P. K. & Ashok, N. M. 2012, Bulletin of the Astronomical Society of India, 40, 243
Banerjee, D. P. K., Barber, R. J., Ashok, N. M., & Tennyson, J. 2005, ApJL, 627, L141
Banerjee, D. P. K., Su, K. Y. L., Misselt, K. A., & Ashok, N. M. 2006, ApJL, 644, L57
Bond, H. E. 2006, The Astronomer's Telegram, 966, 1
Bond, H. E., Henden, A., Levay, Z. G., et al. 2003, Nature, 422, 405
Bonneau, D., Clausse, J.-M., Delfosse, X., et al. 2006, A&A, 456, 789
Chelli, A., Utrera, O. H., & Duvert, G. 2009, A&A, 502, 705
Chesneau, O. 2007, New A Rev., 51, 666
Desidera, S. & Munari, U. 2002, IAU Circ., 7982, 1
Evans, A., Geballe, T. R., Rushton, M. T., et al. 2003, MNRAS, 343, 1054
Exter, K., Cox, N. L. J., Decin, L., & De Beck, E. 2014, in Asymmetrical Planetary Nebulae VI conference, Proceedings of the conference held 4-8 November, 2013. Edited by C. Morisset, G. Delgado-Inglada and S. Torres-Peimbert.
Geballe, T. R., Rushton, M. T., Eyres, S. P. S., et al. 2007, A&A, 467, 269
Haubois, X., Perrin, G., Lacour, S., et al. 2009, A&A, 508, 923
Kamiński, T., Tylenda, R., & Deguchi, S. 2011, A&A, 529, A48
Kolka, I., Liimets, T., Kankare, E., Pursimo, T., & Datson, J. 2009, The Astronomer's Telegram, 2211, 1

Lançon, A. & Wood, P. R. 2000, VizieR Online Data Catalog, 414, 60217
Lane, B. F., Retter, A., Thompson, R. R., & Eisner, J. A. 2005, ApJL, 622, L137
Leinert, C., van Boekel, R., Waters, L. B. F. M., et al. 2004, A&A, 423, 537
Loebman, S. R., Wisniewski, S. J., Schmidt, A. F., et al. in press, ApJ
Lynch, D. K., Rudy, R. J., Russell, R. W., et al. 2004, ApJ, 607, 460
Meilland, A., Kanaan, S., Borges Fernandes, M., et al. 2010, A&A, 512, A73
Millour, F., Chesneau, O., Borges Fernandes, M., et al. 2009, A&A, 507, 317
Millour, F., Meilland, A., Chesneau, O., et al. 2011, A&A, 526, A107
Munari, U., Corradi, R. L. M., Henden, A., et al. 2007, A&A, 474, 585
Munari, U., Desidera, S., & Henden, A. 2002, IAU Circ., 8005, 2
Munari, U., Henden, A., Vallenari, A., et al. 2005, A&A, 434, 1107
Nicholls, C. P., Melis, C., Soszyński, I., et al. 2013, MNRAS, 431, L33
Petrov, R. G., Malbet, F., Weigelt, G., et al. 2007, A&A, 464, 1
Plets, H., Waelkens, C., & Trams, N. R. 1995, A&A, 293, 363
Soker, N. & Tylenda, R. 2003, ApJL, 582, L105
Sparks, W. B., Bond, H. E., Cracraft, M., et al. 2008, AJ, 135, 605
Tatulli, E., Millour, F., Chelli, A., et al. 2007, A&A, 464, 29
Tylenda, R. 2005, A&A, 436, 1009
Tylenda, R. & Kamiński, T. 2012, A&A, 548, A23
Tylenda, R., Kamiński, T., & Schmidt, M. 2009, A&A, 503, 899
Tylenda, R. & Soker, N. 2006, A&A, 451, 223
Tylenda, R., Soker, N., & Szczerba, R. 2005, A&A, 441, 1099
Wagner, R. M. & Starrfield, S. G. 2002, IAU Circ., 7992, 2
Wisniewski, J. P., Bjorkman, K. S., & Magalhães, A. M. 2003a, ApJL, 598, L43
Wisniewski, J. P., Clampin, M., Bjorkman, K. S., & Barry, R. K. 2008, ApJL, 683, L171
Wisniewski, J. P., Morrison, N. D., Bjorkman, K. S., et al. 2003b, ApJ, 588, 486

Appendix A: Bad 2012 calibrator: a newly discovered binary star

The selected calibrator for the 2012 observations, HD 45299, is a previously-unseen visual binary star (see Fig. A.1) that we detect at 16.0 mas separation, position angle (P.A.) $-67°$ and 0.6/0.4 relative fluxes.
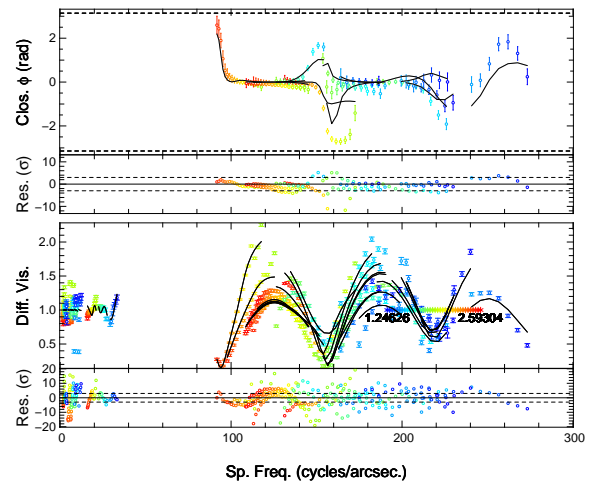

Fig. A.1. AMBER closure phases and differential visibilities (no calibrated V^2 available) for HD45299 (color points with error bars) together with a best-fit model of a binary star (black lines). The spatial frequencies are projected along the binary direction $(-67°)$ to show the binary modulation.